Toxicology Research

PAPER

Cite this: *Toxicol. Res.*, 2015, **4**, 948

Metabolomic profiling of emodin-induced cytotoxicity in human liver cells and mechanistic study†

Xiaoyan Liu,[a,b] Yanqiu Liu,[c] Yang Qu,[a] Mengchun Cheng[a] and Hongbin Xiao*[a,d]

Received 23rd December 2014,
Accepted 23rd March 2015

DOI: 10.1039/c4tx00246f

www.rsc.org/toxicology

Emodin is one of the most representative natural anthraquinone polyphenols and the liver is one of the major target organs for drug-induced toxicology. The hepatocyte is frequently affected due to its role in emodin metabolism and accumulation. Although the hepatotoxicity of emodin has been reported, its toxicological mechanism is still unclear. The purpose of the present study was to evaluate the cytotoxicity of emodin in cultured human normal liver cells (L-02), to investigate the toxicity-related metabolic pathways and to predict the possible toxicity mechanism. Cell viability was analyzed by 3-(4,5-dimethylthiazol-2-yl)-2,5-diphenyltetrazolium bromide (MTT) assay. Cytotoxicity tests demonstrated a concentration-dependent toxic effect of emodin on L-02 cells. Cells were treated for 48 h with low, medium and high doses of emodin, respectively, and then subjected to metabolomics analysis using ultra-high performance liquid chromatography-tandem mass spectrometry (UPLC-MS). Intracellular metabolomics analysis revealed that emodin significantly disturbed cellular glutathione and fatty acid metabolism. In addition, an emodin–cysteine adduct was identified in cell culture medium, and its level increased with increasing concentrations of emodin. The possible relationship among metabolic disorders, adduct formation and emodin hepatotoxicity was also discussed. This study provides new insight into the cytotoxicity of emodin on metabolic pathways in human liver cells.

1 Introduction

Emodin, a natural anthraquinone polyphenol distributed in several popular Chinese herbal medicines including *Rheum palmatum*, *Polygonum multiflorum*, *Cassia acutifolia* and *Aloe vera*, has a wide range of therapeutic applications, including as an anti-diabetic agent in type 2 diabetes[1,2] and as an anticancer agent in various cancers such as pancreatic, *etc.*[3,4] However, side-effects of emodin, such as genotoxicity,[5,6] embryonic toxicity[7] and nephrotoxicity,[8] have been reported in the past few decades. Moreover, it has been revealed to cause *in vivo* hepatotoxicity.[9,10]

Using well-designed *in vitro* assays is now an efficient approach for predicting the toxicity of chemicals to humans, which facilitates understanding the mechanism of the mode of action. In previous studies, the cytotoxicity of chemicals such as perfluorooctanoic acid and pyrrolizidine has been researched in human liver cells.[11,12] Emodin-induced cell injury has been shown to be caused by disruption of mitochondrial function,[13] regulation of protein kinase C expression[14,15] and induction of DNA damage.[16] However, only a few studies focus on the mechanism of emodin-induced hepatocyte cytotoxicity. A recent study revealed that accumulation of emodin in the hepatocyte cytoplasm could contribute to hepatocyte injury.[17]

Drug-induced cytotoxicity is related to cell metabolism. Metabolomics is an omics technology that enables cellular functions to be analyzed *via* a holistic view of metabolic pathways. Of several metabolic detection techniques, liquid chromatography-mass spectrometry (LC-MS) suits the simultaneous profiling of lipid-related metabolic pathways, *e.g.*, fatty acids, steroids, phospholipids and acylcarnitine pathways.[18,19] In this study, an UPLC-MS-based metabolomics approach was applied to the study of emodin-disturbed hepatocyte metabolism. L-02, one of the commonly used human normal liver cell lines for *in vitro* evaluation of cytotoxicity induced by drugs, was chosen as the model system to evaluate the hepatotoxicity of emodin.

[a]*Dalian Institute of Chemical Physics, Chinese Academy of Sciences, 457 Zhongshan Road, Dalian 116023, China*
[b]*University of Chinese Academy of Sciences, Beijing 100049, China*
[c]*College (Institute) of Integrative Medicine, Dalian Medical University, Dalian 116044, China*
[d]*Beijing University of Chinese Medicine, Beijing, 100029, China.*
E-mail: hbxiao69@163.com; Fax: +86 411 8437 9667; Tel: +86 411 8437 9756
†Electronic supplementary information (ESI) available. See DOI: 10.1039/c4tx00246f

Ma and colleagues, and some other researchers' studies, showed that this cell line is suitable for the analysis of drug-induced hepatotoxicity.[20–22]

The primary goal of this study was to investigate emodin-induced cytotoxicity in human normal liver cells (L-02), to assess the toxicity-related metabolic pathways and to explore toxicity-related mechanisms. Cell viability was determined using the MTT assay. After cultivation for 48 h with different doses of emodin (low, medium and high), respectively, the intracellular metabolites in cell samples were extracted for subsequent metabolomic study, and the corresponding cell culture medium was prepared for emodin–cysteine adduct analysis. The formation of an emodin–cysteine adduct in liver cells may contribute to emodin-induced metabolic disorder. Our findings provide insights into the mechanism of emodin-induced hepatotoxicity, and are potentially of clinical significance for the diagnosis of emodin-induced hepatotoxicity.

2 Materials and methods

2.1 Materials

Methanol and acetonitrile (HPLC grade) were obtained from Sigma-Aldrich (St. Louis, MO, USA). Formic acid (HPLC grade) was purchased from Kemiou (Tianjin, China). Roswell Park Memorial Institute-1640 (RPMI-1640) medium and fetal bovine serum (FBS) were obtained from Gibco (Grand Island, NY, USA). 3-(4,5-Dimethylthiazol-2-yl)-2,5-diphenyltetrazolium bromide (MTT), dimethylsulfoxide (DMSO) and a Bradford protein measurement kit were purchased from Solarbio (Beijing, China). Emodin (CAS No. 518-82-1, 98% purity), was obtained from the National Institutes for Food and Drug Control (Beijing, China). Reverse osmosis deionized glass distilled water was obtained in house using a Milli-Q system with a 0.22 μm Millipore filter (Millipore, USA).

2.2 Cell culture

Human normal liver cells (L-02; obtained from Shanghai Obio Biotech. Corp., Ltd., Shanghai, China) were cultured at 37 °C in RPMI-1640 medium supplemented with 10% FBS in a humidified 5% CO_2 atmosphere. The cells were detached using cell scrapers for metabolomics experiments.[23]

2.3 Cell viability assay

An MTT assay was used to measure cell viability. Equal numbers of L-02 cells (10^6 ml^{-1}) were seeded into 96-well plates (3 replicates for each concentration). Cells were cultivated for 24 h and were then treated for 48 h with a series of concentrations of emodin in fresh culture medium ranging from 10 to 120 μM, respectively. Cells with non-emodin-containing medium served as a control, and medium without cells served as the blank. Then, 15 μl of MTT (5 mg ml^{-1}) was added to each well and incubation was continued for 4 h at 37 °C. After discarding the medium, the formazan products were dissolved with 150 μl DMSO and the optical density (OD) values at 570 nm were determined using a Sunrise micro plate absorbance reader (TECAN. Austria). Inhibition rates of emodin were calculated using following equation, and the inhibition ratio curve of emodin was depicted using Graphpad Prism (version 5.0, Intuitive Software for Science, San Diego, CA, USA) accordingly.

$$\text{Inhibition rate} = (\text{OD}_{570\text{control}} - \text{OD}_{570\text{dosed}})/(\text{OD}_{570\text{control}} - \text{OD}_{570\text{blank}}) \times 100\%$$

2.4 Assay for intracellular metabolomics study

Equal numbers of L-02 cells (10^6 ml^{-1}, 2 ml) were seeded into 6-well plates (6 replicates for each group). Cells were cultivated for 24 h and were then treated for 48 h with different concentrations (10 μM, 20 μM and 30 μM) of emodin in fresh culture medium. Vehicle-treated cells (treated with medium) served as the control, and blank medium with emodin (without cells) served as the blank. Cells were quenched using 1 ml chilled methanol, washed three times with 50 mM phosphate buffered saline (PBS, pH 7.4), washed once with water to remove saline solution, scrapped by cell scraper, centrifuged at 92*g* for 5 min to obtain cell pellets, and stored at −80 °C until further analysis.

The method of metabolite extraction was as described in previous research with little modification.[23] Briefly, 200 μl of chilled 80% (v/v) methanol solution was added to quench the enzymatic reactions. Cell lysate was prepared by homogenization using a mini-beadbeater 16 (Biospec, USA) (homogenization for 1 min, interval for 20 s, twice), and centrifuged at 4 °C, 20 627*g* for 10 min. The supernatant was dried under vacuum and then reconstituted with 100 μl of 5% acetonitrile. The protein precipitated in each sample was quantified using a Bradford protein measurement kit (Solarbio) according to the manufacturer's instructions. The total protein contents were used to calibrate the slight differences in the number of cells among different groups. A quality control (QC) sample was prepared by mixing 20 μl aliquots of each sample. The samples were stored at −80 °C prior to LC-MS analysis.

The UPLC-MS analysis was carried out using an Agilent 1290 ultra-performance liquid chromatography system coupled with Agilent 6520 time-of-flight mass spectrometry, using a Zorbax Eclipse plus C18 column (RRHD 1.8 μm, 3.0 × 150 mm; Agilent, USA). The column temperature was maintained at 50 °C, and the injection volume was 5 μl. The separation was performed using a gradient program with water (solvent A, modified by the addition of 0.1% formic acid) and acetonitrile (solvent B). The pump flow rate was 0.3 ml min^{-1} with an initial solvent composition of 5% B. The gradient was conducted from 5–50% B over 3 min, 50–100% B over 3–15 min, held at 100% B for 5 min, decreased to 5% B within 1 min, and held at 5% B for 5 min. To ensure the repeatability and stability of the instrument, the QC sample was analyzed twice prior to the first injection, and analyzed once every eight sample injections during the analysis process. All samples were injected randomly.

Mass spectrometry and accurate mass acquisition were operated in electrospray ionization mode. The optimal capillary voltage and the cone voltage were set at 3.5 kV and 40 V, respectively. The nebulization gas flow rate was set at 8 l min^{-1} and the liquid nebulizer was set at 40 psig. The capillary temperature was set at 350 °C. Data were acquired at a rate of 1 spectrum per second for MS and 3 spectra per second for MS/MS (centroid mode). The collision energy for MS/MS was 10, 20 or 40 eV, according to the properties of metabolites. The mass scan range was from 100 to 1000 for MS and 30 to 1000 for MS/MS. The real-time correction method was used to increase the accuracy and stability of the masses.

2.5 Emodin-cysteine analysis and identification

The cell culture medium was centrifuged at 1467*g* for 10 min to remove debris. Two-hundred microliter aliquots of cell culture medium were taken into 1.5 ml centrifuge tubes. Then, 400 μl of acetonitrile was added, and the mixture was oscillated for 5 min, stood for 30 min at 4 °C and centrifuged at 20 627*g* for 10 min to remove protein. The supernatant was dried under vacuum and reconstituted with 100 μl of 5% acetonitrile. A quality control (QC) sample was prepared by mixing 20 μl aliquots of each sample to ensure the stability of the instrument. The instrumental analysis method was identical with that described in section 2.4. The identification of the emodin–cysteine adduct was based on accurate mass matching, explanation of MS/MS fragments and chemical synthesis result comparison.

2.6 Analysis of metabolomics data

Raw data were analyzed using XCMS online,[24] which follows typical data processing steps, including peak discrimination, peak filtering, peak alignment, noise elimination and the generation of a matrix that consisted of the retention time, *m*/*z* value and the peak areas. Peak areas were first calibrated by protein quantification coefficient to eliminate cell number interference and then normalized by probabilistic quotient normalization (PQN), log transformation and Pareto scaling to make features more comparable. Variables, whose CV% (coefficients of variation) were more than 30% (CV% were calculated based on QC data), were removed from further statistical analysis.[25]

Pattern recognition analysis (principal component analysis, PCA; partial least squares discriminate analysis, PLS-DA) was carried out using SIMCA-P 11.0 software (Umetrics, Sweden). Student's *t*-test (two-tailed) was used for statistical comparisons. The relative concentrations of differential metabolites were expressed in a heatmap. Data analysis and heatmap visualization were conducted using Graphpad Prism version 5.0 and MeV software (version 4.9.0, Dana-Farber Cancer Institute, Boston, MA, USA), respectively.

The identification of the significant metabolites was performed based on a published identification strategy.[26] The following steps were carried out. First, the quasimolecular ions were confirmed according to an extracted ions chromatogram (EIC). Second, the exact masses of monoisotopic molecular weights were used to search our in-house human metabolites fluid database and the free online databases, including METLIN (http://metlin.scripps.edu), HMDB (http://www.hmdb.ca/), ChemSpider (http://www.chemspider.com), KEGG (http://www.genome.jp) and Lipid Maps (http://www.lipidmaps.org). The mass tolerance was set as 10 ppm, and several candidates could be selected for each quasimolecular ion. The third step was to determine the exact structure of each biomarker metabolite through comparison with commercial standards or MS/MS spectral analysis and spectral database comparison.

3 Results

3.1 Cell viability

A dose-dependent increase in L-02 cell inhibition rates was observed with increasing emodin concentrations (ESM_1). The IC_{50} value was calculated as 30 μM on treatment for 48 h using Graphpad prism 5.0. Therefore, the doses used in this study were set as 10, 20, 30 μM (low, medium and high doses); higher doses could induce a death rate larger than 50% of the cells and smaller cell sample would cause larger deviations for further analysis. The morphologies of the adherent L-02 cells after exposure to 10, 20, 30 μM emodin for 48 h are shown in ESM_2. Untreated L-02 cells appeared to have spindle-like shapes and be in high density distribution in the flasks, while L-02 cells treated with emodin gradually became contracted and rounded, and the density of the adherent cells became lower with increasing emodin concentrations.

3.2 Overview of metabolic profiling

The metabolic profiles of L-02 cells were acquired in both positive and negative ionization modes using UPLC-TOF-MS. A QC sample was used to ensure the quality of the metabolomics data (ESM_3). A good separation between the control and dosed groups was observed when using unsupervised principal component analysis (PCA) (Fig. 1a). Clearer results could be obtained from the score plot of PLS-DA (Fig. 1b) (positive mode, R^2X, 0.719; R^2Y, 0.989; Q^2 (cum), 0.899; negative mode, R^2X, 0.872; R^2Y, 0.98; Q^2 (cum), 0.967). These results indicated distinct metabolic differences between the control and emodin-treated groups.

According to variable importance in the projection (VIP) values obtained from PLS-DA models, 80 features in positive mode and 30 features in negative mode were selected as potential cytotoxicity-related biomarkers. After manual validation, 23 features were found as isotope ions. Finally, 28 features (26 metabolites) were identified and semi-quantified (Table S1,† Fig. 2a and ESM_4).

To further analyze emodin hepatotoxicity related metabolic pathways, hierarchical clustering and correlation analysis were performed on identified biomarkers. Interestingly, almost all the marker metabolites showed a consistent pattern of change on low, medium and high dose treatments (Fig. 2b), which indicated the metabolic relevance of these biomarkers. In

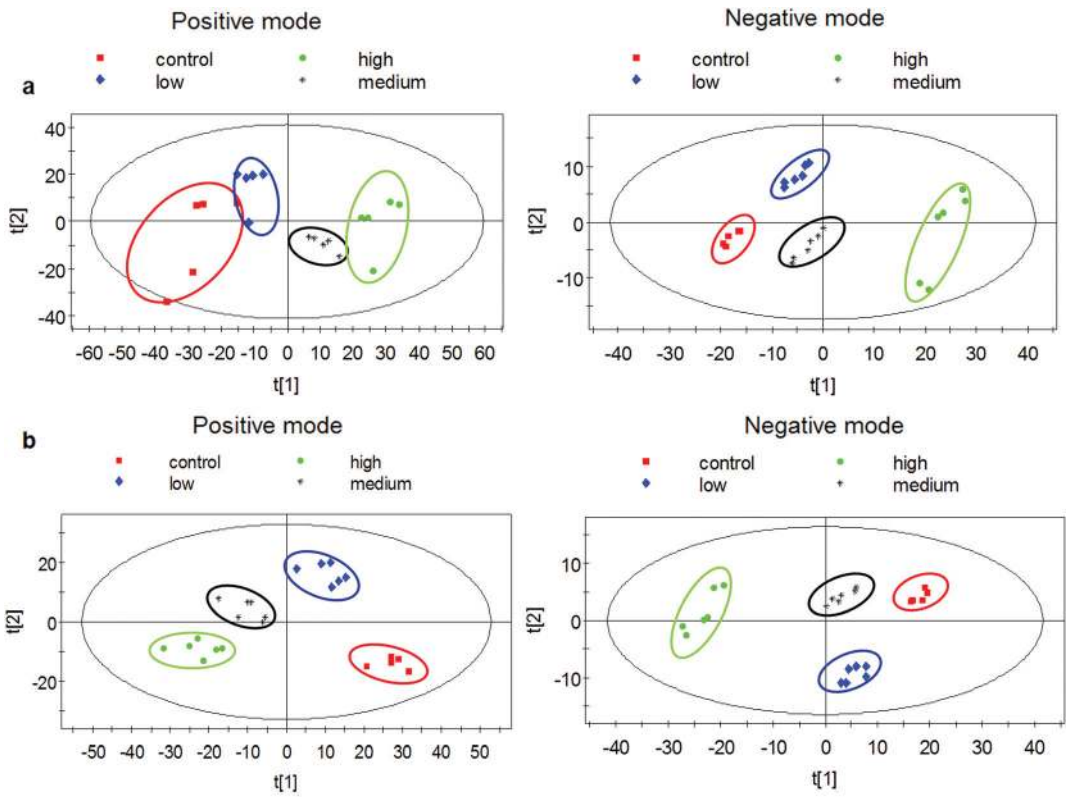

Fig. 1 Metabolomic profiles of the control and emodin-treated groups in positive and negative mode using the UPLC-MS system. (a) PCA scatter plot. (b) PLS-DA scatter plot (positive mode, R^2X, 0.719; R^2Y, 0.989; Q^2 (cum), 0.899; negative mode, R^2X, 0.872; R^2Y, 0.98; Q^2 (cum), 0.967). The artwork was created using SIMCA-P 11.0 software (Umetrics, Sweden).

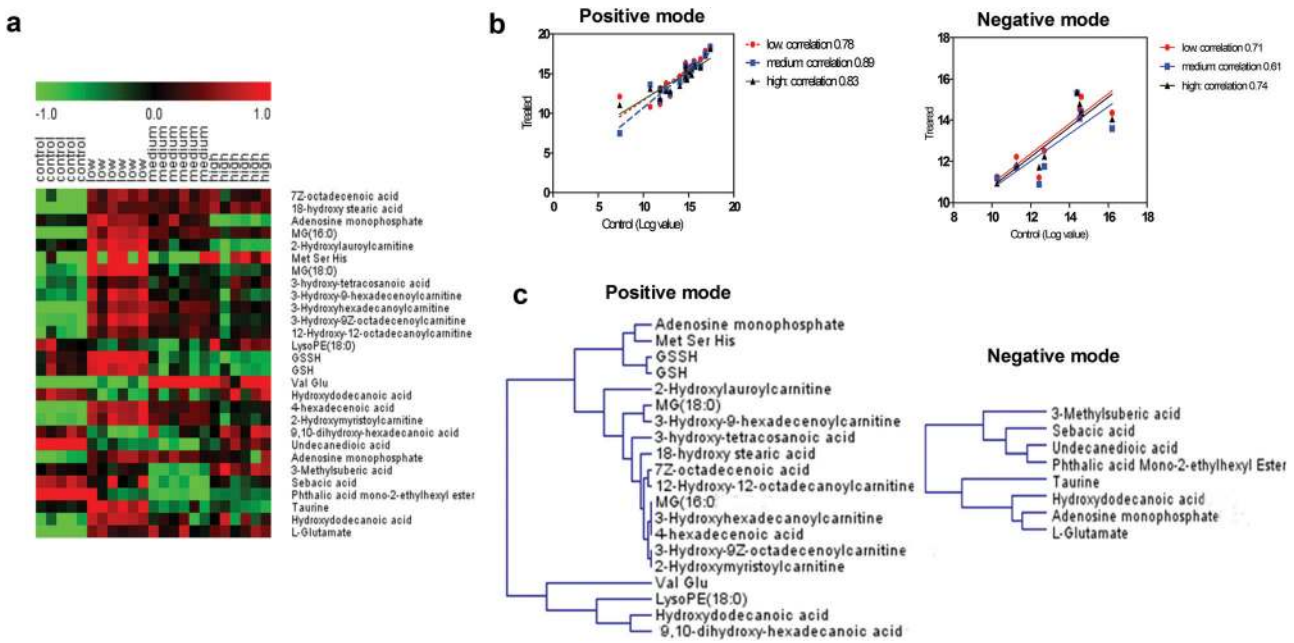

Fig. 2 Significantly changed metabolites in emodin-treated liver cells. (a) Heat map showing differential metabolites in emodin treated liver cells relative to control liver cells. (b) Correlation plots for metabolites altered at low, medium and high doses of emodin treatment in L-02 cells. (c) Dendrogram representing hierarchical clustering of the emodin toxicity related metabolites described in panel a. The heat map and dendrogram were created using MeV software (version 4.9.0, Dana-Farber Cancer Institute, Boston, MA, USA), and correlation plots were plotted using Graphpad Prism (version 5.0, Intuitive Software for Science, San Diego, CA, USA).

addition, hierarchical clustering analysis further ensured the metabolic relevance (Fig. 2c).

3.2.1 Changes in glutathione metabolism. Emodin caused glutathione metabolism disorder in L-02, marked by decreased levels of glutathione (GSH) and oxidized glutathione (GSSH), and an increased level of the metabolite of GSH, glutamate (Fig. 3a). The levels of glutathione-related metabolites gradually decreased or increased with increasing emodin concentration, and at the highest concentration point, the change ranges of metabolites became small when compared to the medium dose group (Fig. 3a). These results suggested that a drastic disturbance of GSH metabolism occurred on emodin treatment and the degree of emodin-induced injury would gradually reach a maximum with increasing concentration of emodin. GSH is a critical cellular antioxidant. After GSH depletion, the toxicity of drugs and chemicals is enhanced.[27] Oxidative stress and peroxidation will subsequently happen, resulting from GSH depletion. Moreover, cellular energy metabolism was also affected by emodin treatment; an increased level of adenosine monophosphate (AMP) suggested an increased ATP utilization in cells.[28]

3.2.2 Changes in fatty acid metabolism. Fatty acid metabolism disorders, including fatty acid oxidation and acylcarnitine metabolism, occurred in L-02 cells with emodin cytotoxicity. Under normal conditions, long-chain fatty acid oxidation involves several steps as follows: the first step is the oxidation of the fatty acid by acyl-CoA-dehydrogenase; the enzyme catalyzes the formation of a double bond. The next step is the hydration of the double bond. The third step is the oxidation of hydroxyacyl-CoA by NAD^+; this process converts the hydroxyl group into an aldehyde group. The final step is the formation of dicarboxylic acid and the cleavage of ketoacyl CoA by the thiol group of another molecule of CoA. However, these normal metabolic processes were disturbed by emodin. The levels of hydroxylated fatty acids, including hydroxydodecanoic acid, 18-hydroxy stearic acid, 9,10-dihydroxy-hexadecanoic acid and 3-hydroxy-tetracosanoic acid gradually increased with increasing emodin concentration. These results prompted

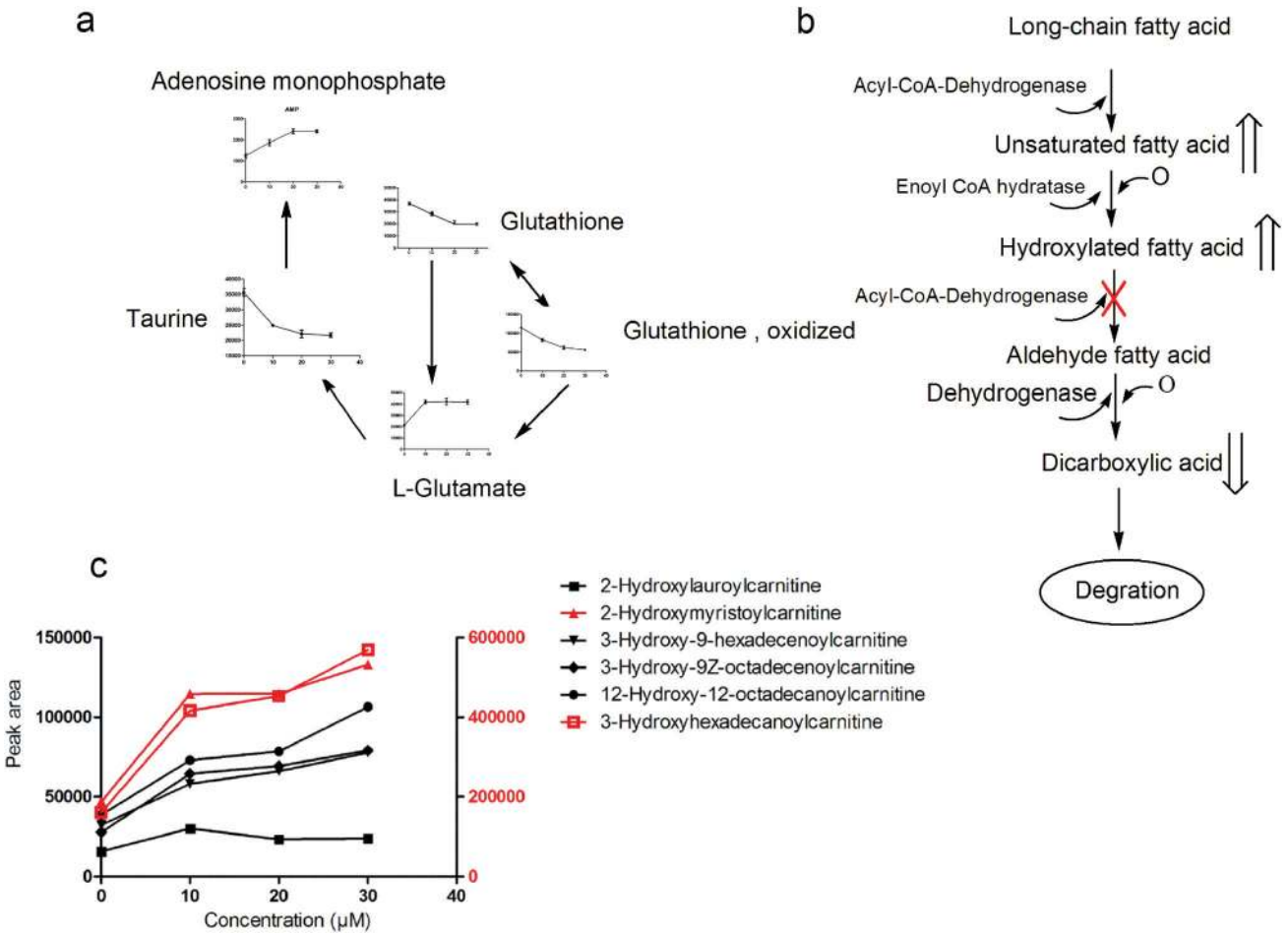

Fig. 3 Disturbance of metabolic pathways induced by emodin. (a) Changes of metabolites in glutathione metabolism. (b) Disturbance of fatty acid oxidation induced by emodin (the double arrow represents increased or decreased levels of the metabolites). (c) Changes of metabolites in acylcarnitine metabolism.

us to predict that the third step of the fatty acid oxidation process was blocked by emodin treatment. This speculation was verified by the increased levels of metabolites, including 4-hexadecenoic acid and 7*Z*-octadecenoic acid, produced in the first oxidation step, and the decreased levels of metabolites produced in the latter step, including undecanedioic acid and sebacic acid (Fig. 3b).

In addition, significant changes of acylcarnitines in emodin treated groups further validated the deduction that fatty acid metabolism disorder occurred in L-02 cells. After emodin treatment, levels of acylcarnitines showed statistically significant increases (Fig. 3c). Acylcarnitines are essential for fatty acid metabolism. They help the activated long-chain fatty acids to be transported into mitochondria and then be oxidized to acetyl-CoA. Moreover, as specific substrates of mitochondrial β-oxidation, acylcarnitines play an important role in mitochondrial function, and mitochondrial dysfunction is reported to be associated with hepatotoxicity.[29] Acylcarnitines can facilitate the transfer of long-chain fatty acids from the cytoplasm into mitochondria during the oxidation of fatty acids, and their levels are the rate-limiting step in fatty acid β-oxidation.[30,31] Our current results suggested that emodin had the potential to disturb fatty acid metabolism in L-02 cells by affecting fatty acid transportation and oxidation in liver cells.

3.3 Emodin–cysteine formation and identification

An emodin–cysteine adduct was identified in cell culture medium (Fig. 4a). Fragment ions of 301.02, 273.02 and 245.04 are the characteristic fragments of emodin and the fragment of 120.01 is the characteristic fragment of cysteine. The structure of this adduct was further validated by comparison with a standard obtained by chemical synthesis, using DMSO as the solubilizing agent. The detailed synthesis procedure is given in ESI† (ESM_5). The level of the emodin–cysteine adduct increased with increasing emodin concentration (Fig. 4b and 4c). Since the CV% of the adduct peak area in the QC data was less than 30% (CV, 7.5%), the differences among different groups were more likely to reflect biological changes rather than analytical variations. However, emodin–cysteine was not detected in blank medium (medium without liver cells) with different concentrations of emodin (Fig. 4b), nor was it detected within L-02 cells. These results suggested that the emodin–cysteine adduct was initially formed within liver cells and then secreted into the culture medium. The formation of this adduct would result in the depletion of intracellular cysteine, which is an essential material for GSH synthesis. GSH synthesis disorder (Fig. 4c) would contribute to a series of cellular metabolic disorders, including in oxidative stress and fatty acid metabolism. Taken together, the formation of the emodin–cysteine adduct was suspected to be related to emodin induced hepatotoxicity.

4 Discussion

The UPLC-MS metabolome analysis demonstrated that emodin had the potential to disturb GSH and fatty acid metabolism in human liver cells, which produced hepatotoxicity. The discovery of a new adduct, emodin–cysteine, facilitated us to propose one mechanism related to emodin-induced hepatotoxicity.

The liver is the essential organ for metabolism of drugs and xenobiotics. Drug-induced hepatotoxicity can result from the

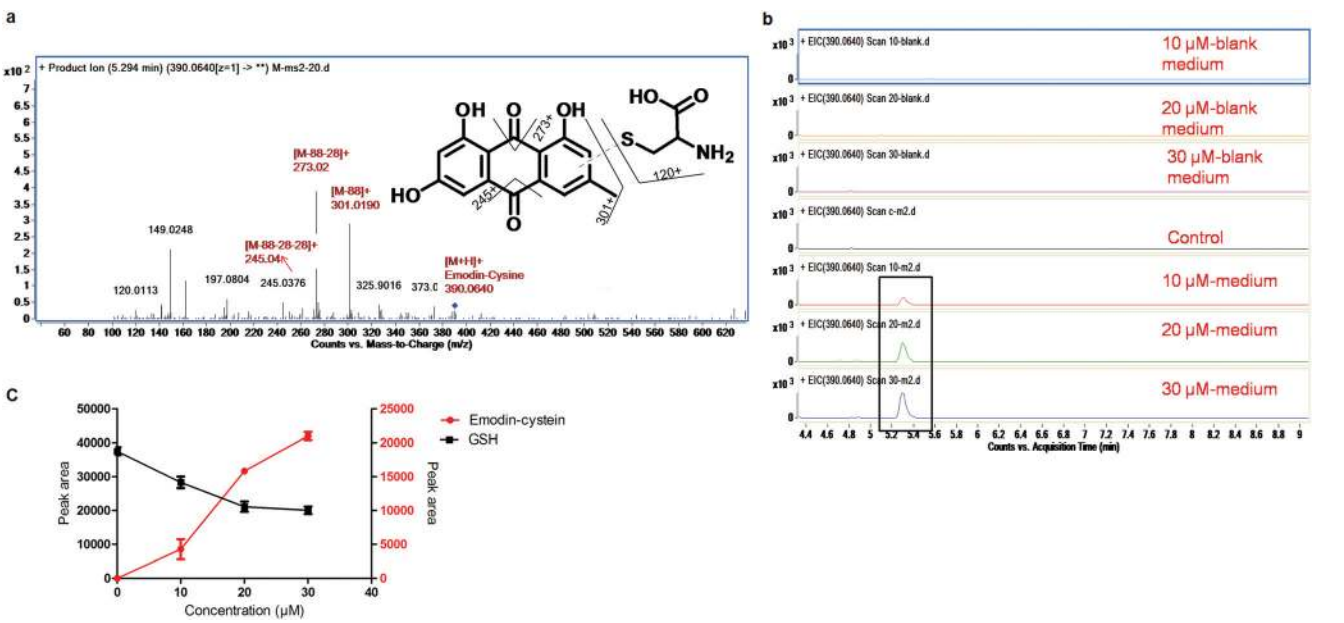

Fig. 4 Emodin–cysteine adduct analysis and identification. (a) MS^2 fragmentation of emodin–cysteine. (b) Extracted ion chromatogram of the emodin–cysteine adduct. (c) Dose-dependent changes of glutathione (GSH) and the emodin–cysteine adduct.

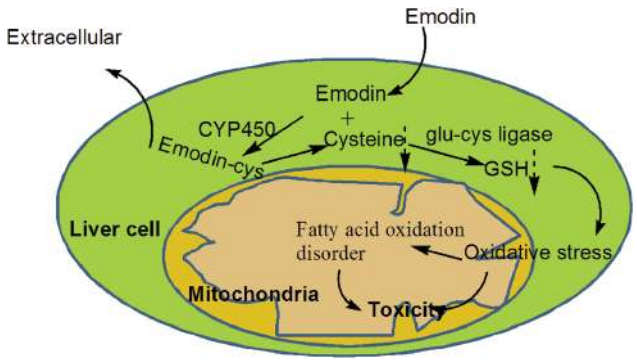

Fig. 5 Probable toxicity mechanism of emodin in liver cells. The dotted arrows represent the up- or down-regulation of metabolites.

direct toxicity of the parent compound or the indirect toxicity of more active metabolites. For example, acetaminophen hepatotoxicity begins with metabolism of the parent compound to the reactive electrophile *N*-acetyl-*p*-benzoquinone imine (NAPQI). Then NAPQI depletes GSH and produces hepatotoxicity.[32,33] Ethanol hepatotoxicity begins with reactive oxygen species (ROS) produced in CYP2E1-dependent ethanol metabolism.[34] The mechanism of emodin hepatotoxicity is rarely reported. The present study suggested an indirect toxicity mechanism of emodin. Emodin is first drawn into the liver cells and binds to cysteine through the function of thioltransferase. Emodin links to cysteine to form a cysteine adduct, which is then released to the culture medium. This combination will 'spend' cellular cysteine, which is a necessary metabolite for glutathione (GSH) synthesis. GSH synthesis plays a central role in cell protection, and GSH depletion will cause a series of metabolic disorders, including oxidative stress and fatty acid oxidation disorder. In addition, synthesis of some proteins containing cysteine will be blocked due to cysteine depletion. All these series of metabolic disorders will consequently contribute to the death of liver cells (Fig. 5).

The limitation of our study is that we only detected emodin–cysteine adduct in the culture medium. However, it must exist within liver cells for a certain period of time, since it cannot be formed in blank culture medium. Therefore, capturing the initial formation of the adduct remains to be investigated. Nevertheless, the results in the present study will help with better understanding of the mechanism of emodin induced hepatotoxicity. Also, several intracellular metabolites and the emodin–cysteine adduct could be used as biomarkers for emodin hepatotoxicity.

5 Concluding remarks

In conclusion, the present study identified emodin hepatotoxicity related metabolic pathways, including GSH metabolism and fatty acid metabolism and discovered a new emodin–cysteine adduct formed in liver cells. A new indirect toxicity mechanism of emodin was proposed. As far as we know, there is no study that has investigated the changes in intracellular metabolites during emodin-induced liver cell cytotoxicity. It is highly probable that the formation of an emodin–cysteine adduct is a main reason for metabolic disorders in emodin treated liver cells, which are related to emodin hepatotoxicity.

Conflict of interests

The authors declare no conflict of interests.

Acknowledgements

This work was supported by grants from the National Technology Major Project (2014ZX09304307-001-006).

References

1 J. Xue, W. Ding and Y. Liu, *Fitoterapia*, 2010, **81**, 173–177.
2 Y.-j. Wang, S.-l. Huang, Y. Feng, M.-m. Ning and Y. Leng, *Acta Pharmacol. Sin.*, 2012, **33**, 1195–1203.
3 Q. Huang, G. Lu, H.-M. Sben, M. C. M. Cbung and C. N. Ong, *Med. Res. Rev.*, 2007, **27**, 609–630.
4 J.-X. Liu, J.-H. Zhang, H.-H. Li, F.-J. Lai, K.-J. Chen, H. Chen, J. Luo, H.-C. Guo, Z.-H. Wang and S.-Z. Lin, *Oncol. Rep.*, 2012, **28**, 1991–1996.
5 S. O. Mueller, I. Eckert, W. K. Lutz and H. Stopper, *Mutat. Res.*, 1996, **371**, 165–173.
6 Y.-Y. Chen, S.-Y. Chiang, J.-G. Lin, J.-S. Yang, Y.-S. Ma, C.-L. Liao, T.-Y. Lai, N.-Y. Tang and J.-G. Chung, *Anticancer Res.*, 2010, **30**, 945–951.
7 M.-H. Chang, F.-J. Huang and W.-H. Chan, *Toxicology*, 2012, **299**, 25–32.
8 B. H. Ali, S. Al-Salam, I. S. Al Husseini, I. Al-Lawati, M. Waly, J. Yasin, M. Fahim and A. Nemmar, *Fundam. Clin. Pharmacol.*, 2013, **27**, 192–200.
9 X. Wu, X. Chen, Q. Huang, D. Fang, G. Li and G. Zhang, *Fitoterapia*, 2012, **83**, 469–475.
10 J. Yu, J. Xie, X.-j. Mao, M.-j. Wang, N. Li, J. Wang, G.-t. Zhaori and R.-h. Zhao, *J. Ethnopharmacol.*, 2011, **137**, 1291–1299.
11 S. Peng, L. Yan, J. Zhang, Z. Wang, M. Tian and H. Shen, *J. Pharm. Biomed. Anal.*, 2013, **86**, 56–64.
12 A. Xiong, F. Yang, L. Fang, L. Yang, Y. He, Y. Y.-J. Wan, Y. Xu, M. Qi, X. Wang, K. Yu, K. W.-K. Tsim and Z. Wang, *Chem. Res. Toxicol.*, 2014, **27**, 775–786.
13 Z. Huang, G. Chen and P. Shi, *Arch. Pharmacal Res.*, 2008, **31**, 742–748.
14 H. Z. Lee, *Br. J. Pharmacol.*, 2001, **134**, 1093–1103.
15 M. Acevedo-Duncan, C. Russell, S. Patel and R. Patel, *Int. Immunopharmacol.*, 2004, **4**, 1775–1784.
16 Y.-Y. Chen, S.-Y. Chiang, J.-G. Lin, Y.-S. Ma, C.-L. Liao, S.-W. Weng, T.-Y. Lai and J.-G. Chung, *Int. J. Oncol.*, 2010, **36**, 1113–1120.

17 C.-L. Li, J. Ma, L. Zheng, H.-J. Li and P. Li, *J. Pharm. Biomed. Anal.*, 2012, **71**, 71–78.
18 E. Gonzalez, S. van Lmpd, J. Conde-Vancells, V. Gutierrez-de Juan, M. Perez-Cormenzana, R. Mayo, A. Berisa, C. Alonso, C. A. Marquez, J. Barr, S. C. Lu, J. M. Mato and J. M. Falcon-Perez, *Metabolomics*, 2012, **8**, 997–1011.
19 B. S. Kumar, B. C. Chung, O.-S. Kwon and B. H. Jung, *J. Appl. Toxicol.*, 2012, **32**, 505–520.
20 X.-m. Chen, J. Liu, T. Wang and J. Shang, *Toxicol. in Vitro*, 2012, **26**, 649–655.
21 M. Ma, Z. Jiang, J. Ruan, X. Tan, J. Liu, C. Wang, X. M. Zha and L. Zhang, *Exp. Toxicol. Pathol.*, 2012, **64**, 611–618.
22 L. L. Ji, M. Zhang, Y. C. Sheng and Z. T. Wang, *Toxicol. in Vitro*, 2005, **19**, 41–46.
23 K. Dettmer, N. Nuernberger, H. Kaspar, M. A. Gruber, M. F. Almstetter and P. J. Oefner, *Anal. Bioanal. Chem.*, 2011, **399**, 1127–1139.
24 R. Tautenhahn, G. J. Patti, D. Rinehart and G. Siuzdak, *Anal. Chem.*, 2012, **84**, 5035–5039.
25 E. C. Chan, K. K. Pasikanti and J. K. Nicholson, *Nat. Protocols*, 2011, **6**, 1483–1499.
26 J. Chen, X. Zhao, J. Fritsche, P. Yin, P. Schmitt-Kopplin, W. Wang, X. Lu, H. U. Haring, E. D. Schleicher, R. Lehmann and G. Xu, *Anal. Chem.*, 2008, **80**, 1280–1289.
27 X. Fu, T. S. Chen, M. B. Ray, H. T. Nagasawa and W. M. Williams, *J. Biochem. Mol. Toxicol.*, 2004, **18**, 154–161.
28 H. Sakagami, M. Sugimoto, S. Tanaka, H. Onuma, S. Ota, M. Kaneko, T. Soga and M. Tomita, *Metabolomics*, 2014, **10**, 270–279.
29 X. Shi, D. Yao, B. A. Gosnell and C. Chen, *J. Lipid Res.*, 2012, **53**, 2318–2330.
30 D. S. Roe, B. Z. Yang, C. Vianey-Saban, E. Struys, L. Sweetman and C. R. Roe, *Mol. Genet. Metab.*, 2006, **87**, 40–47.
31 J. G. Okun, S. Kolker, A. Schulze, D. Kohlmuller, K. Olgemoller, M. Lindner, G. F. Hoffmann, R. J. A. Wanders and E. Mayatepek, *Biochim. Biophys. Acta, Mol. Cell Biol. Lipids*, 2002, **1584**, 91–98.
32 M. R. McGill, C. D. Williams, Y. Xie, A. Ramachandran and H. Jaeschke, *Toxicol. Appl. Pharmacol.*, 2012, **264**, 387–394.
33 J. G. Diaz Ochoa, J. Bucher, A. R. R. Pery, J. M. Zaldivar Comenges, J. Niklas and K. Mauch, *Front. Pharmacol.*, 2012, **3**, 204–204.
34 G. J. G. Hartmut Jaeschke, A. I. Cederbaum, J. A. Hinson, D. Pessayre and J. J. Lemasters, *Toxicol. Sci.*, 2002, **65**, 166–176.